34th Annual International Conference of the IEEE EMBS
San Diego, California USA, 28 August - 1 September, 2012

Quantitative Investigative Analysis of Tumour Separability in the Prostate Gland using Ultra-high b-value Computed Diffusion Imaging

Jeffrey Glaister, Andrew Cameron, Alexander Wong, Masoom A. Haider

Abstract— **High b-value diffusion-weighted imaging is a promising approach for diagnosing and localizing cancer in the prostate gland. However, ultra-high b-value imaging is difficult to achieve at a high signal-to-noise ratio due to hardware limitations. An alternative approach being recently discussed is computed diffusion-weighted imaging, which allows for estimation of ultra-high b-value images from a set of diffusion-weighted acquisitions with different magnetic gradient strengths. This paper presents a quantitative investigative analysis of the improvement in tumour separability in the prostate gland from using ultra-high b-value computed diffusion-weighted imaging. The analysis computes ultra-high b-value images for six patient cases and investigates the separability of the tumour from the normal prostate gland. Based on quantitative metrics such as expected probability of classification error and the Receiver Operating Characteristic (ROC), it was found that the use of ultra-high computed diffusion-weighted imaging may significantly improve tumour separability, with a b-value around 3000 providing optimal separability.**

I. Introduction

With 913,000 new diagnoses in 2008, prostate cancer is the second most common type of cancer in males [1]. Furthermore, an estimated 258,000 deaths globally that same year were from prostate cancer, making it the sixth leading cause of death from cancer in males [1]. However, the prognosis is excellent with a relative 5-year survival rate of 100% for cancer in the local stage, if detected early [2]. The localization of prostate cancer is particularly important for treatment using minimally-invasive focal therapy technologies. Therefore, there is significant interest in improving the detection and localization of prostate cancer for improving prostate cancer management and treatment.

One promising imaging modality for detecting and localizing prostate cancer is diffusion-weighted magnetic resonance imaging. Diffusion-weighted imaging (DWI) detects differences in the diffusion of water molecules. This can be used to differentiate between normal and tumour tissues in the prostate gland. To obtain diffusion-weighted MRI images, a diffusion gradient is applied, which has a strength quantified by its b-value. Different b-values are used to acquire a set of diffusion-weighted MRI images. Using this set of images, the apparent diffusion coefficient (ADC) values are estimated for the different tissue types present. The ADC value measures the diffusion properties of the tissue and is different in prostate tumours compared to normal tissue due to restricted diffusion in tumours. The ADC values are commonly estimated using least-squares or maximum likelihood strategies, and can be used to detect and localize tumours [3].

Another approach to identify prostate cancer using diffusion-weighted imaging is to use a gradient with a high b-value during image acquisition [4], [5], [6]. This approach can in theory be very promising for locating tumours within the prostate gland because at high b-values, tumours exhibit higher signal intensities and thus could be more distinct from normal tissue. However, due to hardware limitations, ultra-high b-value imaging is difficult to achieve at a high signal-to-noise ratio. This makes it difficult to attain quality ultra-high b-value acquisitions for diagnostic purposes [7]. To overcome these physical hardware limitations, the concept of computed diffusion-weighted imaging was recently introduced, where a set of diffusion-weighted image acquisitions with different magnetic gradient strengths are used to estimate higher b-value images [8]. The generated images have much higher signal-to-noise ratios than if acquisitions were made at those high b-values, and as such are more useful to radiologists for diagnostic purposes. Given that the concept of computed diffusion-weighted imaging is very recent, there is very limited investigation into the appropriateness of this approach for prostate cancer diagnosis.

This paper presents a quantitative investigative study into determining whether tumours exhibit greater separability in the prostate gland when using ultra-high b-value computed diffusion imaging, as well as determining which b-values are most appropriate for improving tumour separability in the prostate gland. To the authors' knowledge, a study on quantifying the separability of tumour in the prostate gland using computed b-value diffusion-weighted imaging for multiple patient cases has not been performed before. Previous studies that focus on prostate cancer have provided only preliminary findings on the contrast-to-noise ratio gained from computed high b-value diffusion-weighted imaging using a single patient case, but have not provided a comprehensive analysis of tumour separability from ultra-high b-value imaging across multiple cases [9]. The study presented in this paper aims to provide a more complete, quantitative picture on the benefits of ultra-high b-value computed diffusion imaging for prostate diagnosis.

This paper is organized as follows. In Section II, the methodologies of computing ultra-high b-value computed

This work was supported by the Natural Sciences and Engineering Research Council of Canada and the Ontario Ministry of Economic Development and Innovation.

Jeffrey Glaister, Andrew Cameron, and Alexander Wong are with Department of Systems Design Engineering, University of Waterloo, Ontario, Canada, N2L 3G1. {a4camero,jlglaist,a28wong}@uwaterloo.ca

Masoom A. Haider is with the the Department of Medical Imaging, Princess Margaret Hospital and the University Health Network, University of Toronto, Canada, M5S 1A1. m.haider@utoronto.ca

diffusion-weighted imaging are presented. In Section III, the testing methodologies of the presented study are outlined and in section IV, results quantifying tumour separability across multiple patient cases are presented. Finally, conclusions are drawn and future directions are discussed in Section V.

II. Computed Diffusion-Weighted Image Methodology

This section presents the methodologies for performing ultra-high b-value computed diffusion-weighted imaging from a Bayesian estimation perspective, which can be described as follows. First, the ADC value corresponding to a tissue type is estimated using a set of diffusion-weighted images measured with different b-values. The relationship between b-values and ADC value is assumed to be mono-exponential and is given in Eq. 5, where A is the ADC value, b_i is the b-value associated with signal intensity S_i, and S_α is the reference signal intensity associated with b_α. This equation is readily solved for A.

$$S_i = S_\alpha e^{-(b_i - b_\alpha)A} \tag{1}$$

If a collection of DWI measurements is used instead, the ADC estimation problem can be formulated as a Bayesian estimation problem (Eq. 2), where S is the collection of DWI measurements, A is the ADC, and $P(\cdot|A)$ is the conditional probability given A.

$$\hat{A} = \arg\max_A P(S|A). \tag{2}$$

Furthermore, assuming the measurements S to be statistically independent, the probability can be expressed as shown in Eq. 3, where S_i is a single DWI measurement.

$$P(S|A) = \prod_i P(S_i|A). \tag{3}$$

The conditional probability of S_i given A is assumed in Eq. 4.

$$P(S_i|A) \overset{\text{iid}}{\sim} \mathcal{N}(S_\alpha e^{-(b_i - b_\alpha)A}, \sigma^2) \tag{4}$$

Once A has been estimated, the estimate $\hat{A}$ may be used to obtain computed diffusion-weighted images $\hat{S}_i$ at any desired value of b_i according to:

$$\hat{S}_i = S_\alpha e^{-(b_i - b_\alpha)\hat{A}} \tag{5}$$

III. Testing Methodology

We used two main measures of performance in our experiments. Details about the image acquisition protocols, theoretical formulations of our performance metrics, and experimental results follow.

TABLE I: Summary of patients with DWI taken with 2 b-values $\{100, 1000$ s/mm$^2\}$.

	Age	DFOV (cm^2)	Resolution (mm^3)	TE (ms)	TR (ms)
1	79	24×24	$1.36 \times 1.36 \times 4$	67	4876
2	60	24×24	$1.36 \times 1.36 \times 4$	67	3336
3	59	24×24	$1.36 \times 1.36 \times 4$	67	3336

TABLE II: Summary of patients with DWI taken with 4 b-values $\{50, 75, 100, 1000$ s/mm$^2\}$.

	Age	DFOV (cm^2)	Resolution (mm^3)	TE (ms)	TR (ms)
4	67	24×24	$1.67 \times 1.67 \times 3.5$	61	4118
5	80	24×24	$1.67 \times 1.67 \times 3.5$	61	4890
6	77	24×24	$1.67 \times 1.67 \times 3.5$	61	4890

A. Image acquisition protocol

All MRI acquisitions used in this analysis were obtained using a Philips Achieva 3.0T machine at Sunnybrook Health Sciences Centre, Toronto, Canada. Information about the six patient datasets used here is summarized in Tables I and II, including Displayed Field of View (DFOV), echo time (TE), and repetition time (TR). Images were processed in the ProCanVAS (Prostate Cancer Visual Analysis System) platform developed at the University of Waterloo Vision and Image Processing research group.

B. Testing metrics

For each patient case, the ADC was estimated and the estimate was used to generate diffusion-weighted images at a variety of b-values. We measured tumour separability using the expected probability of error and Receiver Operating Characteristic (ROC) curves for a linear classifier.

The expected probability of error is given by

$$P(\varepsilon) = \int_{-\infty}^{\infty} \min(p(tumour|x),\, p(healthy|x))p(x)\, dx. \tag{6}$$

Unlike statistical tests such as the t-test, this measure avoids making assumptions about the probability distribution of the noise, instead estimating the error directly from the measurements.

The posteriors $p(\cdot|x)$ were calculated using Bayes' Theorem,

$$p(\cdot|x) = \frac{p(x|\cdot)p(\cdot)}{p(x)}, \tag{7}$$

as we were given ground truth. The histograms of each region were used to generate estimates for the likelihoods $p(x|\cdot)$, while the region sizes were used to calculate the priors $p(\cdot)$.

ROC curves visualize the separability of two classes, without the need to explicitly select a threshold [10]. The threshold is varied, and the prostate pixels are classified as tumour or normal prostate based on pixel intensity. Each threshold segmentation result is compared with the manually segmented ground truth, and the true positive rate (TPR) and false positive rate (FPR) are calculated. The equations for TPR and FPR are shown in Eq. 8 and 9.

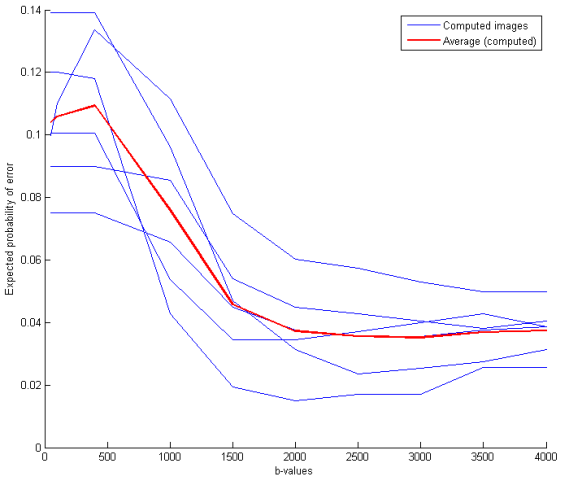

Fig. 1: The expected probability of error curves suggest improvements for a wide range of b-values past 1500, with an optimal choice in the neighbourhood of 3000.

$$TPR = \frac{\text{true positives}}{\text{total positives}} \tag{8}$$

$$FPR = \frac{\text{false positives}}{\text{total negatives}} \tag{9}$$

The ROC curve plots TPR vs. FPR. An ideal ROC curve passes through the upper left point $(0, 1)$, which corresponds to a FPR of 0 and TPR of 1.

IV. Experimental Results

A. Expected probability of error

Fig. 1 shows the results of calculating $P(\varepsilon)$ for the images generated at each b-value, along with their mean. As the b-value of the computed images increases, the separability of tumour from healthy tissue tends to improve until it reaches a plateau in the neighbourhood of $b = 3000$. This implies that tumour segmentation can be more accurate with these high b-value computed images.

B. Visual comparison

Examples of high-b value images are shown in Fig. 2 to 4. Computed images are shown for b-values of 100, 1000, 3000 and 4000. Measured images are also shown for b-values of 100 and 1000. As the b-value increases, the tumour becomes brighter, while the rest of the prostate darkens. Visually, it becomes easier to distinguish tumour from normal prostate in computed high b-value images, such as b-values of 4000.

C. ROC Curves

Sets of ROC curves for three patients are shown in Fig. 5 to 7, which correspond to the prostate images shown. The ROC curves for different b-values are plotted on the same axis to better compare separability in high b-value images. As the b-value increases, the ROC curve moves towards the upper left quadrant, corresponding to a decrease in the FPR and increase in the TPR for optimal thresholds. This means that the tumour in the image is able to be more accurately segmented. The curves for the original measured images with b-values of 100 and 1000 are also displayed on the same axis, which perform worse than computed b-value images. Similar trends were seen in the curves for other patients.

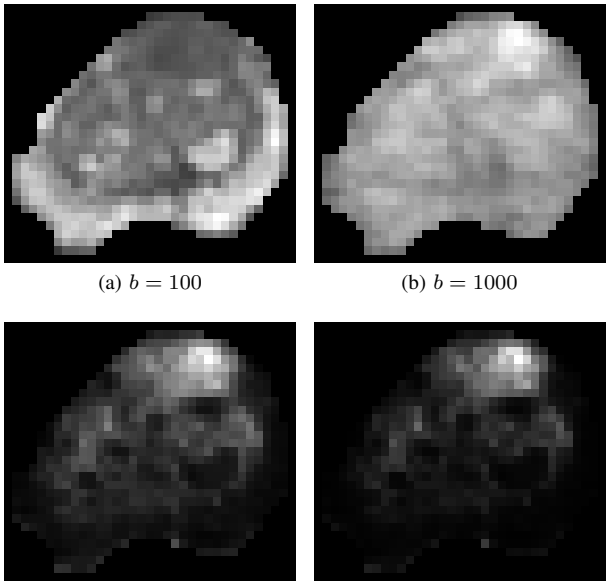

(a) $b = 100$ (b) $b = 1000$

(c) $b = 3000$ (d) $b = 4000$

Fig. 2: Patient case 3: observed diffusion-weighted images for lower b-values (a, b) and computed diffusion-weighted images for higher b-values (c, d). The cancerous tissue stands out in the computed, high b-value images.

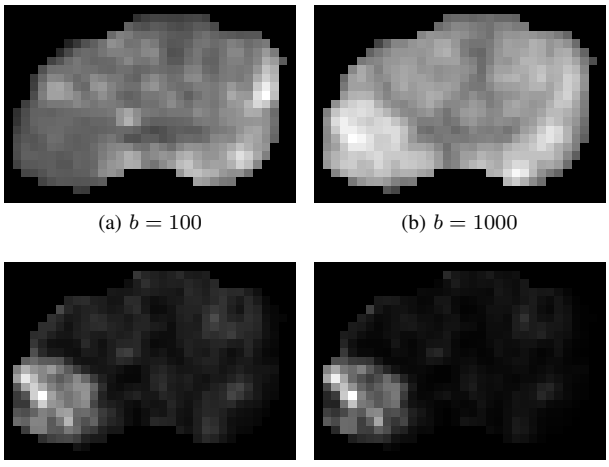

(a) $b = 100$ (b) $b = 1000$

(c) $b = 3000$ (d) $b = 4000$

Fig. 3: Patient case 4: observed diffusion-weighted images for lower b-values (a, b) and computed diffusion-weighted images for higher b-values (c, d).

V. Conclusions

In this paper, a quantitative investigative analysis of the improvement in tumour separability in the prostate gland that can be obtained from ultra-high b-value computed diffusion-weighted imaging. Based on the analysis of six

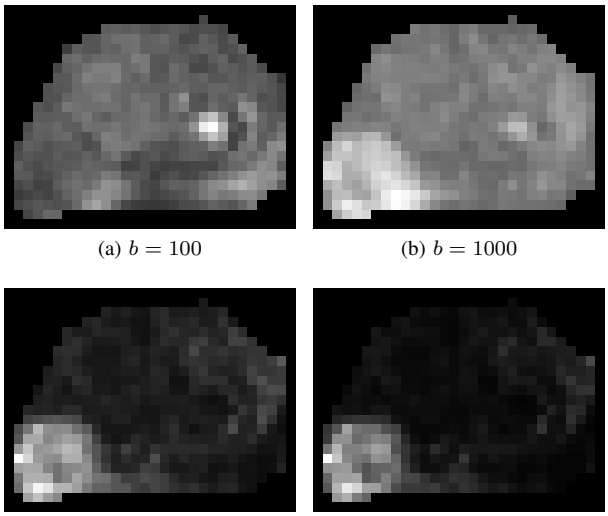

(a) $b = 100$ (b) $b = 1000$

(c) $b = 3000$ (d) $b = 4000$

Fig. 4: Patient case 5: observed diffusion-weighted images for lower b-values (a, b) and computed diffusion-weighted images for higher b-values (c, d).

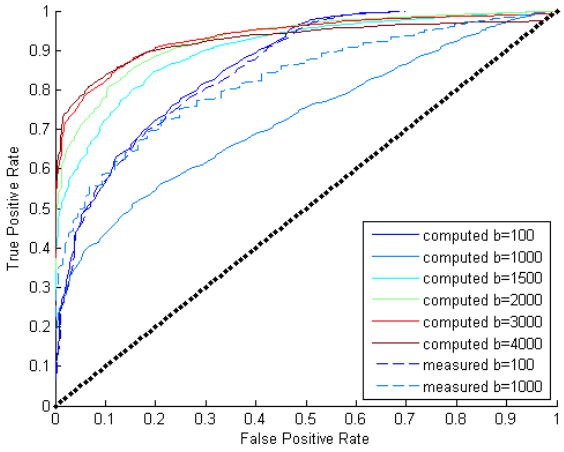

Fig. 5: ROC curve for patient case 3, showing good classification performance for higher b-value computed images.

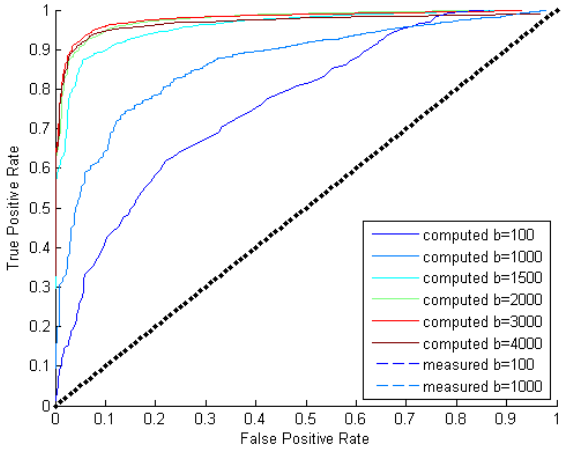

Fig. 6: ROC curve for patient case 4.

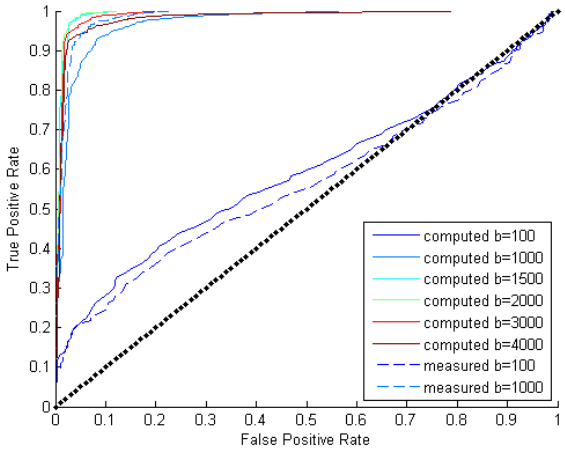

Fig. 7: ROC curve for patient case 5.

patient cases using quantitative metrics for separability, it was demonstrated that the use of ultra-high computed diffusion-weighted imaging holds great potential for significantly improving tumour separability, which can be crucial in the design of computerized prostate cancer diagnosis systems. Future directions include investigating alternative approaches for performing ultra-high b-value computed diffusion-weighted imaging for further improving tumour separability, as well as computerized schemes for localizing prostate cancer using such an approach.

REFERENCES

[1] A. Jemal, F. Bray, M. M. Center, J. Ferlay, E. Ward, and D. Forman, *Global Cancer Statistics*, CA: A Cancer Journal for Clinicians, vol. 61, iss. 2, pp. 69-90, March 2011.

[2] A. Jemal, R. Siegel, E. Ward, Y. Hao, J. Xu, T. Murray, and M. J. Thun, *Cancer Statistics, 2008*, CA: A Cancer Journal for Clinicians, vol. 58, iss. 2, pp. 71-96, March 2008.

[3] S. Walker-Samuel, M. Orton, L. D. McPhail, and S. P. Robinson, *Robust Estimation of the Apparent Diffusion Coefficient (ADC) in Heterogeneous Solid Tumors*, Magnetic Resonance in Medicine, vol. 62, iss. 2, pp. 420-429, August 2009.

[4] C. K. Kim, B. K. Park, and B. Kim, *High-b-Value Diffusion-Weighted Imaging at 3 T to Detect Prostate Cancer: Comparisons Between b Values of 1,000 and 2,000 s/mm^2*, American Journal of Roentgenology, vol. 194, no. 1, pp. 33-37, January 2010.

[5] K. Katahira et al., *Ultra-high-b-value diffusion-weighted MR imaging for the detection of prostate cancer: evaluation in 201 cases with histopathological correlation*, European Radiology, vol. 21, no. 1, pp. 188-196, January 2011.

[6] J. Absil, N. Hottat, T. Metens, and C. Matos, *Diffusion-weighted imaging of the prostate at 3T using high b-factors*, Proceedings 16th Scientific Meeting of International Society for Magnetic Resonance in Medicine, pp. 2762, May 2008.

[7] K. Kitajima, Y. Kaji, K. Kuroda, and K. Sugimura, *High b-value diffusion-weighted imaging in normal and malignant peripheral zone tissue of the prostate: effect of signal-to-noise ratio.*, Magnetic Resonance in Medical Sciences, vol. 7, no. 2, pp. 93-99, 2008.

[8] M. D. Blackledge, M. O. Leach, D. J. Collins, and D. Koh, *Computed Diffusion-weighted MR Imaging May Improve Tumor Detection*, Radiology, vol. 261, iss. 2, pp. 573-581, November 2011.

[9] M. C. Maas, J. J. Fütterer, and T. W. Scheenen, *Contrast-to-noise ratio in extrapolated and measured high b-value diffusion weighted prostate MR images*, Proceedings 19th Scientific Meeting of International Society for Magnetic Resonance in Medicine, pp. 3066, May 2011.

[10] T. Fawcett, *An Introduction to ROC Analysis*, Pattern Recognition Letters, vol. 27, iss. 8, pp. 861-874, 2006.